25.5 A 320GHz Subharmonic-Mixing Coherent Imager in 0.13μm SiGe BiCMOS

Chen Jiang[1], Ali Mostajeran[1], Ruonan Han[2], Mohammad Emadi[3], Hani Sherry[4], Andreia Cathelin[4], Ehsan Afshari[1]

[1]Cornell University, Ithaca, NY,
[2]Massachusetts Institute of Technology, Cambridge, MA,
[3]Qualcomm, San Jose, CA,
[4]STMicroelectronics, Crolles, France

Terahertz imaging has been gaining increasing attention for its emerging applications in security, biomedical and material characterization. Previous works have demonstrated terahertz imagers on silicon: in [1], the authors demonstrated a 280GHz 4×4 array and an 860GHz pixel using Schottky-barrier diodes; in [2], a 0.7-to-1.1THz 1k-pixel camera was presented. Unfortunately, most previous works are based on incoherent direct detection (Fig. 25.5.1), which causes low sensitivity due to the output droping quickly with input power ($\propto V_{RF}^2$), and, as a result, need exceedingly high power sources for illumination. This problem can be alleviated by utilizing coherent heterodyne detection scheme (Fig. 25.5.1), in which the terahertz input (RF) mixes with a local oscillation (LO) signal and generates an output with the amplitude proportional to $V_{RF}V_{LO}$. As the LO power is normally significantly higher than RF, the sensitivity is much enhanced. Moreover, as the output also carries the RF phase information (φ_{RF}), digital beamforming is achievable. For a better comparison, an NPN transistor is configured both as a direct detector (input power injected from the emitter) and a heterodyne detector (-20dBm LO power pumped into the base). The simulated output current with different input power is shown in Fig. 25.5.1, in which we observe a sensitivity enhancement of more than 40dB. However, this coherent sensing scheme introduces a great challenge of synchronizing the frequencies of the transmitter (TX) radiated signal and the receiver (RX) LO. Fortunately, phase-locked terahertz sources have been demonstrated on silicon [3,4]. In this paper, a fully integrated 320GHz high-sensitivity coherent-imaging transceiver chipset is demonstrated.

The TX could be divided into two parts: a 4×4 320GHz radiator array and a 160GHz PLL (Fig. 25.5.2). The return-path-gap-based oscillator structure is adopted in the radiator cells (Fig. 25.5.2) since it can maximize the oscillation activity, eliminate the 2nd-harmonic self-power-cancelation/loading effect and efficiently radiate the 2nd-harmonic signal [3]. With these, the radiators achieve high output power and DC-to-radiation efficiency. Within each row, 4 radiators are mutually coupled together. To ensure frequency coherency between TX and RX, each row of the radiators are inject-locked by the mutually locked VCOs through the 2nd-harmonic buffers (Fig. 25.5.2). Unfortunately, due to the large oscillation activity in the radiators, the locking range between the radiators and VCOs is small. However, a sufficient locking range is needed for the TX to be immune from the environmental change during the imaging process. Focusing on this issue, we achieved better locking range compared with [3]. A large tuning range is also required for the PLL in order to cover the radiator frequency shift caused by inaccurate device models at high frequency and process variation. In simulations, we achieved ~17GHz tuning range at the 160GHz output of the PLL, which is enough to cover ±5.3% radiator frequency shift. The simulated radiation pattern is also shown in Fig. 25.5.2. Compared to multiplier-chain-based locked terahertz sources, the PLL-based structure does not need any high frequency off-chip source, thus achieving a higher level of integration and a smaller size.

The RX (Fig. 25.5.3) is composed of an 8-cell detector array and a similar 160GHz PLL as in TX (with only one VCO and the 2nd-harmonic buffer is optimized for delivering LO power). Ideally, we could use the PLL to inject-lock a 320GHz oscillator to deliver the LO power. However, as mentioned before, with a large oscillation activity, the locking range for LO is small. Due to the possible TX/RX frequency mismatch caused by process variation, such small locking range is hardly able to ensure synchronization. To solve this problem, a subharmonic mixing scheme (160GHz LO directly provided by the PLL) is used for its larger LO tuning range as well as simplicity and less TX/RX frequency mismatch due to hardware reuse. A highly symmetric distribution network is designed to deliver the LO power evenly to each detector cell (Fig. 25.5.3). In simulation, a -12dBm LO power is delivered to each cell. The geometry of the employed differential patch antenna is shown in Fig. 25.5.3. The simulated antenna gain is 2.2dB. A detailed block diagram of a detector cell is shown in Fig. 25.5.3. An NPN transistor is used as the nonlinear device to perform LO (pumped in at base) and RF (injected from emitter) mixing. The transistor size is chosen by trading-off the conversion loss, device noise as well as input impedance at the emitter for antenna matching. To alleviate the LO self-mixing problem, a differential structure is adopted. The IF signal is then amplified by a low-noise pre-amplifier before it is mixed again into a 100kHz baseband signal. Finally, a low-pass filter (200kHz cutoff frequency) is followed. The total gain for the baseband circuits is simulated to be 60dB. It is noteworthy that due to the array topology and a phase-preserving detecting scheme, electrical scanning based on RX beam steering is possible and potentially able to significantly reduce imaging time.

Both TX and RX chips are implemented in the 0.13μm SiGe:C BiCMOS technology from STMicroelectronics. The TX output spectrum and the power measurement setups are shown in Fig. 25.5.4. A hemispherical high-resistivity silicon lens is attached to the backside of the chip to eliminate the substrate wave. The measured radiator free-running and locked spectrum as well as locked phase noise are shown in Fig. 25.5.4. Due to the large division ratio and the wide tuning range required for the PLL, the phase noise is slightly sacrificed. The TX output locking range at different radiator V_{Base} is shown in Fig. 25.5.4. As V_{Base} increases, the oscillation activity of the radiators increases, and as discussed before, the locking range decreases quickly. However, a total locking range of 3.91GHz is still achieved. The TX directivity is measured to be 18dBi (radiation pattern shown in Fig. 25.5.4). The calorimeter is located 9cm away from the TX chip during the power measurement in order to ensure a far-field condition. The measured output power as well as the radiator array DC-to-radiation efficiency vs supply voltage are shown in Fig. 25.5.4. The peak EIRP and output power are 21.1dBm and 2.03mW, respectively. The RX measurement setup is shown in Fig. 25.5.5. To eliminate a standing wave caused by a reflection at the RX PCB, an absorber is positioned in front of it. The measured output-signal PSD and the output noise spectrum density are shown in Fig. 25.5.5. Due to limited close-in phase noise of the PLLs (both RF and LO phase noise is determined by the PLLs), the output signal power is spread within the 90kHz bandwidth, however it is still 28dB higher than the noise floor with a 15cm TX-to-RX distance. The output signal is integrated from 10kHz to 100kHz to get an output rms voltage (this operation sacrifices the RF phase information in the output). The output rms voltage as well as the received power of a detector cell vs distance are shown in Fig. 25.5.5. An equivalent incoherent responsivity is defined as the responsivity an incoherent detector needs to generate the same output rms voltage with the same received power. The conversion gain from the input terahertz voltage (assume 50Ω impedance) to the output rms voltage as well as the equivalent responsivity vs distance are shown in Fig. 25.5.5. With the transmission-mode imaging setup shown in Fig. 25.5.1, some terahertz images are formed (Fig. 25.5.6). The performance summaries of TX and RX as well as a comparison table are given in Fig. 25.5.6. To make a fair comparison between coherent and incoherent imagers, a sensitivity is defined as the input power for the output to have SNR=1 within a 1kHz bandwidth (corresponding to 1ms time constant for fast imaging). The comparison shows the coherent imager can achieve ~10× better sensitivity. The sensitivity enhances even further with larger bandwidth (~20× for 10kHz and ~70× for 100kHz) corresponding to faster imaging.

References:

[1] R. Han et al., "Active Terahertz Imaging Using Schottky Diodes in CMOS: Array and 860-GHz Pixel," *IEEE J. Solid-State Circuits,* vol. 48, no. 10, pp. 2296-2308, Oct. 2013.
[2] R. Al Hadi et al., "A 1 k-Pixel Video Camera for 0.7–1.1 Terahertz Imaging Applications in 65-nm CMOS," *IEEE J. Solid-State Circuits,* vol. 47, no. 12, pp. 2999-3012, Dec. 2012.
[3] R. Han et al., "A 320GHz Phase-Locked Transmitter with 3.3mW Radiated Power and 22.5dBm EIRP for Heterodyne THz Imaging Systems," *ISSCC Dig. Tech. Papers,* pp. 446-447, Feb. 2015.
[4] P.-Y. Chiang et al, "A Silicon-Based 0.3 THz Frequency Synthesizer With Wide Locking Range," *IEEE J. Solid-State Circuits,* vol. 49, no. 12, pp. 2951-2963, Dec. 2014.
[5] K. Sengupta et al., "Silicon Integrated 280 GHz Imaging Chipset With 4X4 SiGe Receiver Array and CMOS Source," *IEEE Trans. THz Science and Technology,* vol. 5, no. 3, pp. 427-437, May 2015.
[6] M. Uzunkol et al., "A 0.32 THz SiGe 4x4 Imaging Array Using High-Efficiency On-Chip Antennas," *IEEE J. Solid-State Circuits,* vol. 48, no. 9, pp. 2056-2066, Sept. 2013.

 978-1-4673-9467-3/16/$31.00 ©2016 IEEE

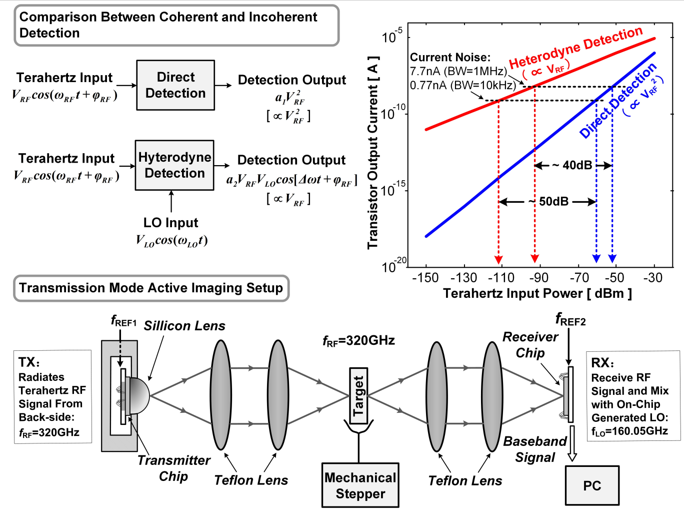

Figure 25.5.1: Coherent heterodyne detection and incoherent direct detection (top left), comparison of simulation results (top right), and transmission mode active imaging setup (bottom).

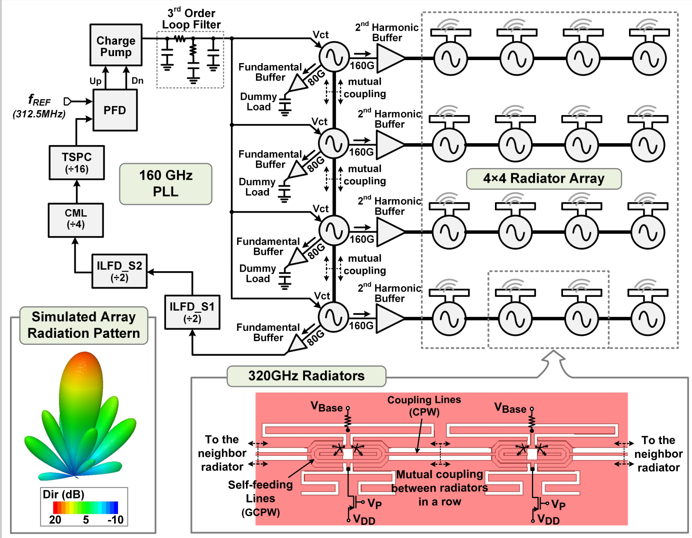

Figure 25.5.2: 320GHz phase-locked transmitter: architecture, radiator cells and simulated radiation pattern.

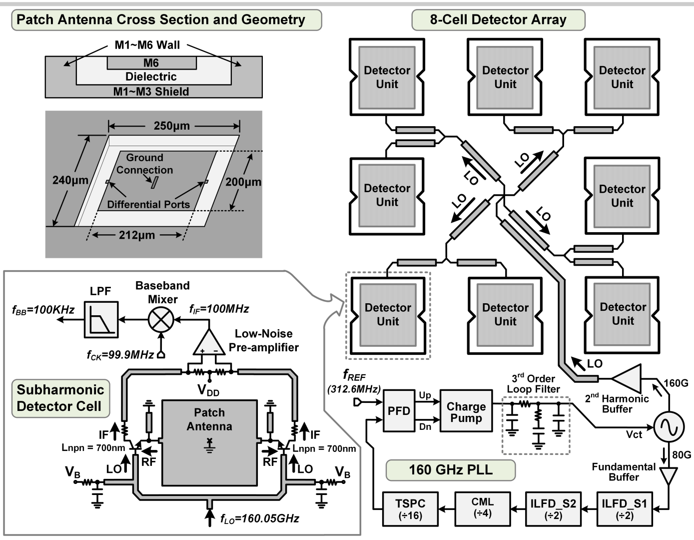

Figure 25.5.3: Subharmonic-mixing coherent receiver: architecture, antenna geometry and single cell block diagram.

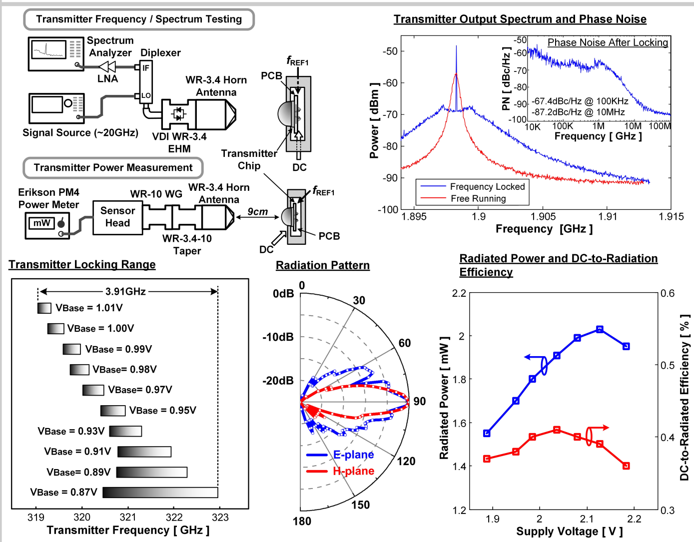

Figure 25.5.4: The transmitter measurement: setup, spectrum, phase noise, locking range, radiation pattern, output power and efficiency.

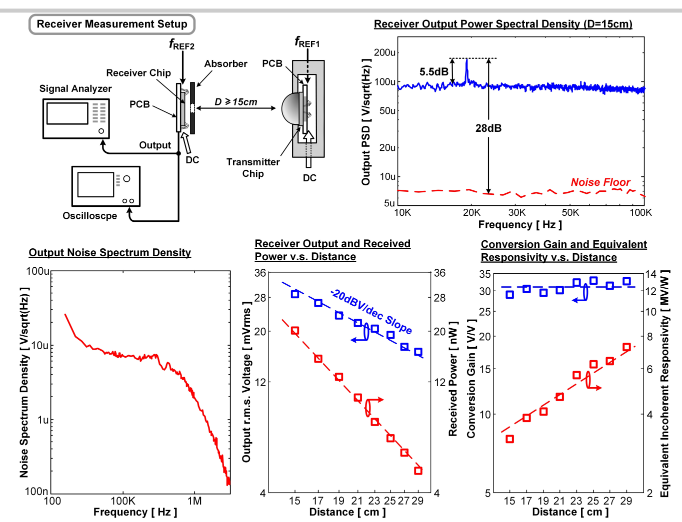

Figure 25.5.5: The receiver measurement: setup, output PSD and noise, output rms voltage and received power, conversion gain and equivalent incoherent responsivity.

Terahertz Images

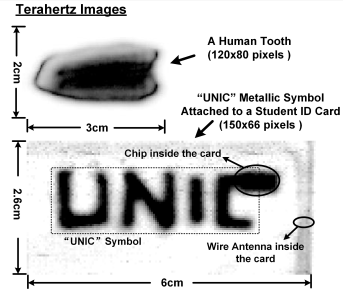

Transmitter Performance Summary

Output Frequency Range (GHz)	319.04 ~ 322.95
Peak Radiated Power (mW)	2.03
Peak EIRP (dBm)	21.1
Directivity (dBi)	18.0
Peak Radiator Efficiency (%)	0.41
Phase Noise (dBc/Hz)	-67.4 @ 100KHz offset -87.2 @ 10MHz offset
DC Consumption (mW)	433 (Radiator Array) 172 (PLL)

Receiver Performance Summary

LO Tuning Range (GHz)	152.5 ~ 164.8
Antenna Gain (dB)	2.2
Output Noise ($\mu V/Hz^{1/2}$)	6.7 @ 100KHz
Conversion Gain (V/V)	31.0
Sensitivity (pW) [1kHz BW]	70.1
DC Consumption (mW)	41.6 (Detector Array) 75.5 (PLL)

Comparison Table

References	Technology	Frequency	Array Size	Responsivity	Sensitivity 6	Coherent
JSSC 2013 [1]	130nm CMOS	0.28 THz	4×4	336 V/W 1	917 pW 7	No
		0.86 THz	single pixel	273 V/W 1	1.33 nW 7	
JSSC 2012 [2]	65nm CMOS	0.86 THz	32×32	140 kV/W 2	3.16 nW 7	No
Tran. THz 2015 [5]	130nm SiGe	0.26 THz	4×4	2.6 MV/W 3	250~278 pW 7	No
JSSC 2013 [6]	180nm SiGe	0.32 THz	4×4	18 kV/W 4	1.08 nW 7	No
This Work	130nm SiGe	0.32 THz	8	> 7.26 MV/W 5	70.1 pW	Yes

1. 24dB on-chip amplifier gain is de-embeded. 2. On-chip readout circuit gain and 5dB off-chip VGA gain included.
3. 33-57.5dB VGA gain included. 4. 22dB amplifier/buffer gain included.
5. The equivalent resonsivity of the coherent detector is defined as: the responsivity an incoherent detector needs to generate same output r.m.s. voltage with the same received power level. 60dB baseband gain included.
6. The sensitivity is defined as the input power level for the output signal to have SNR=1 within 1kHz bandwidth.
7. Assume noise spectrum density is flat within the 1kHz bandwidth.

Figure 25.5.6: Terahertz images, performance summaries and comparison with other state-of-the-art imagers.

25

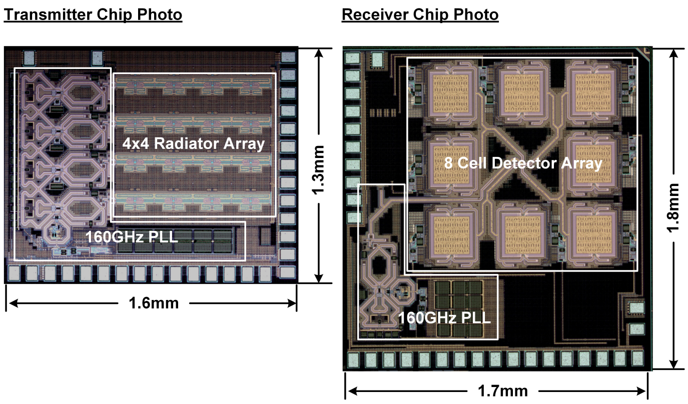

Figure 25.5.7: Transmitter and receiver die micrographs.